

Comparison of synthesized and acquired high *b*-value diffusion-weighted MRI for detection of prostate cancer

Karoline Kallis (PhD)², Christopher C. Conlin (PhD)¹, Allison Y. Zhong², Troy S. Hussain², Aritrick Chatterjee (PhD)^{6, 7}, Gregory S. Karczmar (PhD)^{6, 7}, Rebecca Rakow-Penner (MD, PhD)¹, Anders Dale (PhD)^{1, 3, 4}, Tyler Seibert (MD, PhD)^{1, 2, 5}

¹Department of Radiology, UC San Diego Health, La Jolla, CA, USA

²Department of Radiation Medicine and Applied Sciences, UC San Diego Health, La Jolla, CA, USA

³Department of Neurosciences, UC San Diego Health, La Jolla, CA, USA

⁴Halicioğlu Data Science Institute, UC San Diego, La Jolla, CA, USA

⁵Department of Bioengineering, UC San Diego Jacobs School of Engineering, La Jolla, CA, USA

⁶Department of Radiology, University of Chicago, Chicago, IL, USA

⁷Sanford J. Grossmann Center of Excellence in Prostate Imaging and Image Guided Therapy, University of Chicago, Chicago, IL, USA

Grant Support

This work was supported, in part, by the National Institutes of Health (NIH/NIBIB K08EB026503, NIH UL1TR000100), the American Society for Radiation Oncology, and the Prostate Cancer Foundation.

Disclosures

AMD is a Founder of and holds equity in CorTechs Labs, Inc, and serves on its Scientific Advisory Board. He is a member of the Scientific Advisory Board of Human Longevity, Inc. and receives funding through research agreements with General Electric Healthcare. RRP is a consultant for Human Longevity, Inc. She also receives funding through research grants from GE Healthcare and Imagine Scientific to UC San Diego; she has an equity interest in CorTechs Labs, Inc. and serves on its Scientific Advisory Board. She also has equity interest in CureMetrix. TMS reports honoraria from Multimodal Imaging Services Corporation, Varian Medical Systems, and WebMD; he has an equity interest in CorTechs Labs, Inc. and serves on its Scientific Advisory Board. These companies might potentially benefit from the research results. The terms of the above arrangements have been reviewed and approved by the University of California San Diego in accordance with its conflict-of-interest policies. Drs. Chatterjee and Karczmar report equity in QMIS LLC, outside the submitted work.

*Corresponding Author

Tyler Seibert, PhD

Assistant Professor

Department of Radiation Medicine & Applied Sciences

UC San Diego Health

3855 Health Sciences Drive

La Jolla, CA 92093-0843

(858) 246-0500

tseibert@health.ucsd.edu

Background:

High b -value diffusion-weighted images (DWI) are used for detection of clinically significant prostate cancer (csPCa). To decrease scan time and improve signal-to-noise ratio, high b -value (>1000 s/mm²) images are often synthesized instead of acquired.

Purpose:

Qualitatively and quantitatively compare synthesized DWI (sDWI) to acquired (aDWI) for detection of csPCa.

Study Type:

Retrospective

Subjects:

151 consecutive patients who underwent prostate MRI and biopsy.

Sequence:

Axial DWI with $b=0$, 500, 1000, and 2000 s/mm² using a 3T clinical scanner using a 32-channel phased-array body coil

Assessment:

We synthesized DWI for $b=2000$ s/mm² via extrapolation based on monoexponential decay, using $b=0$ and $b=500$ s/mm² (sDWI₅₀₀) and $b=0$, $b=500$, and $b=1000$ s/mm² (sDWI₁₀₀₀). Differences between sDWI and aDWI were evaluated within regions of interest (ROIs). The maximum DWI value within each ROI was evaluated for prediction of csPCa. Classification accuracy was also compared to Restriction Spectrum Imaging restriction score (RSIrs), a previously validated biomarker based on multi-exponential DWI.

Statistical Tests:

Discrimination of csPCa was evaluated via area under the receiver operating characteristic curve (AUC). Statistical significance was assessed using bootstrap difference (two-sided $\alpha=0.05$).

Results:

Within the prostate, mean \pm standard deviation of percent mean differences between sDWI and aDWI signal were $-46\pm 35\%$ for sDWI₁₀₀₀ and $-67\pm 24\%$ for sDWI₅₀₀. AUC for aDWI, sDWI₅₀₀, sDWI₁₀₀₀, and RSIrs within the prostate 0.62[95% confidence interval: 0.53, 0.71], 0.63[0.54, 0.72], 0.65[0.56, 0.73] and 0.78[0.71, 0.86], respectively. When considering the whole field of view, classification accuracy and qualitative image quality decreased notably for sDWI compared to aDWI and RSIrs.

Data Conclusion:

sDWI is qualitatively comparable to aDWI within the prostate. However, hyperintense artifacts are introduced with sDWI in the surrounding pelvic tissue that interfere with quantitative cancer detection and might mask metastases. In the prostate, RSIrs yields superior quantitative csPCa detection than sDWI or aDWI.

Keywords:

Diffusion-weighted imaging, prostate cancer, synthetic high b -values, Restricted Spectrum Imaging

Abbreviation

DWI	diffusion-weighted imaging
csPCa	clinically significant prostate cancer
FOV	field of view
RSIrs	restriction spectrum imaging restriction score
CNR	contrast-to-noise ratio
sDWI	synthesized diffusion-weighted image
aDWI	acquired diffusion-weighted image
ROI	region of interest
ROC	receiver operating characteristic
AUC	area under the curve
FPR90	false positive rate at 90% sensitivity
SNR	signal to noise ratio

Introduction

Diffusion-weighted imaging (DWI) is a critical component of multiparametric MRI for the detection and characterization of clinically significant prostate cancer (csPCa)¹. The degree of diffusion-weighting in DWI is indicated by the *b*-value, with higher *b*-values corresponding to images with less signal where water in tissues diffuses more rapidly². High *b*-values are used for their greater tumor conspicuity and detection of even small lesions³. The Prostate Imaging – Reporting and Data System (PI-RADS v2.1) recommends the acquisition of high *b*-values (1400–2000 s/mm²) for lesion detection, without precisely defining an optimal value for csPCa⁴. While clinically valuable, high *b*-values require more scan time and suffer from low signal-to-noise ratio (SNR) and increased susceptibility to artifacts due to microscopic motion or small fluctuations in local magnetic field. One common solution, permitted by PI-RADS, is to synthesize high *b*-value images by extrapolating signal from acquired low *b*-value images using a mono-exponential model^{1,5}. However, mono-exponential models do not adequately represent restricted diffusion in complex tissues^{6,7}, possibly calling into question the accuracy of synthesized images.

More advanced DWI models have been developed to better account for tissue microstructure, including intravoxel incoherent motion imaging^{8,9}, diffusion kurtosis imaging^{10,11}, Vascular, Extracellular, and Restricted Diffusion for Cytometry in Tumor (VERDICT)^{12–14}, hybrid

multidimensional MRI (HM-MRI)^{15–18}, and Restriction Spectrum imaging (RSI)^{12,19}. In RSI, the diffusion signal is modeled as a weighted sum of different compartments representing different tissue types^{19,20}. The RSI restriction score (RSIs) is based on the model coefficient for the most restricted diffusion compartment and has been shown to be a useful biomarker for the detection of csPCa^{20–22}.

Studies have yielded contradicting results on whether synthesized *b*-values are clinically interchangeable with acquired DWI (aDWI) images. Liu *et al.*²³ compared various models, including the standard mono-exponential, for the detection of csPCa and concluded that non-linear fitting with various *b*-values is superior to simpler models. In contrast, other studies reported better image quality for synthetic DWI (sDWI) with a similar tumor detection rate in comparison to acquired DWI^{5,24–27}.

In this study, we qualitatively and quantitatively analyzed the differences between acquired and synthesized high *b*-value images for detection of csPCa. Further, we compared the detection rate of csPCa between DWI and RSIs.

Materials and Methods

Patient Cohort

This retrospective study was approved by the institutional review board (IRB 805394). 151 men were included in the study who underwent MRI examination between November 2017 and December 2020. These were consecutive patients scanned with the same protocol and for whom results of a prostate biopsy (performed within 180 days of the MRI) were available. Patient characteristics are summarized in **Table 2**.

For all patients, suspicious lesions were contoured per PI-RADS v2.1 by board-certified radiologists using MIM software (MIM Software, Inc; Cleveland, OH). Whole-gland prostate segmentation was performed using OnQ Prostate software (Cortechs Labs, San Diego, CA, USA). Clinically significant prostate cancer (csPCa) was defined as grade group ≥ 2 . On biopsy,

86 of the 151 patients were found to have csPCa, while 65 had only benign tissue or grade group 1 cancer. In patients who underwent prostatectomy, grade group was determined per final pathology report.

MRI Acquisition

All MRI acquisitions were performed on a 3T clinical GE scanner (Discovery MR750, GE Healthcare, Waukesha, WI, USA) using a 32-channel phased-array body coil surrounding the pelvis. Acquisition parameters are summarized in **Table 1**. A single axial DWI volume was acquired for each patient. T_2 -weighted reference images were acquired for all patients with field of view (FOV) identical to the DWI volume. RSI calculations were performed as described in prior studies^{20–22}.

Post-processing of the image data was performed using in-house software in MATLAB (version R2017a, MathWorks, Natick, MA, USA). DWI images were corrected for B_0 inhomogeneity distortions, gradient nonlinearity, and eddy currents^{28–30}. Multiple acquired DWI samples at specific b -values were averaged together and normalized by median signal intensity of urine in the bladder at $b = 0$ s/mm².

Synthetic b -value Computation

Synthetic high b -value DWI (sDWI) was calculated using the conventional, mono-exponential formula (see below) and using b -values up to 500 s/mm² (sDWI₅₀₀) or b -values up to 1000 s/mm² (sDWI₁₀₀₀).

$$S(b) = S_0 e^{-b ADC}$$

$S(b)$ is DWI signal for a given b -value, b . S_0 is the signal with no diffusion weighting. ADC is the apparent diffusion coefficient. sDWI was calculated for $b=2000$ s/mm² to match the acquired high b -value DWI (aDWI). To explore the application of sDWI and aDWI for detection of significant

cancer lesions outside of the prostate, sDWI and RSIRs were additionally calculated for one representative patient with csPCa and bone metastasis.

Data Analysis

All data analysis was performed using in-house MATLAB scripts (version R2021a, MathWorks, Natick, MA, USA). Quantitative differences between sDWI and aDWI were estimated by a voxel-wise comparison of the images. Relative deviations were calculated for three different regions of interest (ROIs): prostate, prostate plus a margin of 5 mm, and the whole field of view (FOV) using the following formula:

$$\Delta S = \frac{1}{N} \sum_{i=0}^N \frac{S_s - S_a}{S_a}$$

where S_s is the synthetic signal intensity, S_a the acquired signal and N the number of voxels in the considered images. Mean and standard deviation of ΔS over all patients are reported. A negative value indicates that the acquired signal intensity is higher than the synthesized signal intensity. Further, violin plots were generated for the 50th, 95th, and 98th percentile of signal intensity within several ROIs: prostate; prostate plus margin (5 mm, 30 mm, or 70 mm); and the whole FOV. For the whole FOV, values higher than 3000 signal intensity units (SIU) were capped and set to 3000 SIU. Violin plots present the median value in combination with the kernel density distribution ³¹.

Lesion conspicuity was evaluated using the contrast-to-noise ratio (CNR) between lesion and surrounding prostate tissue. CNR is defined as the following:

$$CNR = \frac{(\mu_{lesion} - \mu_{prostate})}{\sqrt{\sigma_{lesion}^2 + \sigma_{prostate}^2}}$$

where μ is the mean signal of the ROI under consideration and σ the standard deviation. CNR was evaluated for all patients and patients diagnosed with csPCa. A higher CNR indicates a better

tumor conspicuity³². Significant differences between CNRs of different images and patient cohorts were tested using two sample t-test with a confidence level of 0.01.

Prediction of whether csPCa was found on biopsy was also evaluated for aDWI, sDWI, and RSIrs. RSIrs is a quantitative cancer biomarker based on a multi-exponential DWI model and has been previously shown to be more accurate than conventional DWI^{20–22}. Computation of RSIrs for this dataset was performed previously and is described in detail in previous publications^{21,22,33}. Briefly, the coefficient for the slowest diffusion compartment (corresponding to intracellular restricted diffusion) was normalized by the median signal within the prostate on $b=0$ s/mm² images. The maximum aDWI, sDWI, or RSIrs value within each considered ROI was used as the predictor variable, as done in previous work²². This is analogous to the maximum standard uptake value (SUV) in quantitative Positron Emission Tomography (PET) imaging. Receiver-operating characteristic (ROC) curves were calculated, and the area under the curve (AUC) reported for aDWI, sDWI, and RSIrs. The false positive rate at 90% sensitivity (FPR90) was also reported for each metric. AUC and FPR90 were compared using bootstrap (N=10,000) 95% confidence intervals and p -values.

Results

Figure 1 shows the difference between acquired and synthesized b -values for a representative patient using the mean signal intensity within the prostate. Within the prostate, mean \pm standard deviation of percent differences between sDWI and aDWI were $-46\pm 35\%$ for sDWI₁₀₀₀ and $-67\pm 24\%$ for sDWI₅₀₀. A negative error indicates sDWI had lower values than aDWI. Comparing sDWI₁₀₀₀ to sDWI₅₀₀, a difference of $-41\pm 4\%$ was estimated (see **Table 3**). sDWI₅₀₀ had overall larger errors than sDWI₁₀₀₀. Signal intensity of aDWI was lower than sDWI in the prostate and in the prostate plus 5 mm margin, as indicated by a negative mean difference and lower median for the 50th, 95th and 98th percentiles. The 50th percentile of aDWI is higher than sDWI for all considered ROIs. For the 95th and 98th percentiles, however, sDWI is larger for

margins of ≥ 30 mm beyond the prostate. The standard deviation of sDWI is larger than that of aDWI for all ROIs and all considered percentiles. Comparison of the 50th, 95th and 98th percentiles for five ROIs is shown in **Figure 3**. Mean and standard deviation of CNR over all patients was 0.95 ± 0.87 , 0.84 ± 0.80 , 0.65 ± 0.66 and 0.97 ± 0.79 for aDWI, sDWI₁₀₀₀, sDWI₅₀₀ and RSIrs, respectively. A lower CNR indicates a lower tumor conspicuity. CNR considering only patients with csPCa changed to 1.00 ± 0.84 , 0.86 ± 0.78 , 0.65 ± 0.65 and 0.99 ± 0.76 for aDWI, sDWI₁₀₀₀, sDWI₅₀₀ and RSIrs respectively. CNR for aDWI and RSIrs proved to be significantly different to sDWI ($p < 0.01$) for all patients and patients with csPCa. **Figure 5** compares sDWI, aDWI and RSIrs for detection of significant cancer lesions outside of the prostate.

For detection of csPCa, the AUCs for sDWI and aDWI were similar in both the prostate and prostate plus 5 mm (**Figure 3** and **Table 4**). Classification accuracy decreased significantly for sDWI when considering the whole FOV (AUC = 0.45 [0.36, 0.54] for sDWI₁₀₀₀ and 0.47 [0.38, 0.56] for sDWI₅₀₀). RSIrs was superior to sDWI and aDWI for all ROIs ($p < 0.01$). The AUC of RSIrs was 0.77 [0.69, 0.84] within prostate plus 5 mm and decreased to 0.70 [0.61, 0.78] for the whole FOV. FPR90 was similar for aDWI and sDWI in all ROIs. Mean FPR90 was significantly lower for RSIrs than for either aDWI or sDWI, indicating fewer false positives ($p < 0.05$).

Discussion

We found that synthesized DWI images can be qualitatively similar to acquired DWI within the prostate even though sDWI is quantitatively an inaccurate representation of aDWI. Moreover, sDWI introduces unacceptable artifacts and inaccuracies in pelvic tissues. sDWI₅₀₀ calculated using only b -values up to 500 s/mm² was inferior to sDWI₁₀₀₀. Acquisitions of an increased number of lower b -values might have the possibility to improve sDWI but would potentially increase the scan time. sDWI proved to be systematically different from aDWI within the prostate and in the whole FOV. Even within the prostate, sDWI and aDWI differed between 55-72%. Nonetheless, within the prostate and the prostate plus 5 mm margin, lesion conspicuity was reasonably

preserved. Both sDWI and aDWI had a similar quantitative performance in detecting csPCa with an AUC ranging between 0.56-0.65. However, sDWI introduced larger errors in the surrounding pelvic tissue even in a reduced FOV acquisition. Overall RSIs outperformed sDWI and aDWI for quantitative prediction of biopsy-proven csPCa for all considered ROIs.

Severe artifacts were observed on sDWI in the pelvic tissue outside of the prostate, in particular for sDWI₅₀₀, which makes the detection of metastasis outside of the prostate region difficult, **Figure 5**. There are many ways to potentially improve the calculation of synthesized images including bi-exponential or multi-exponential modeling²³. For example, RSIs is based on a multi-exponential model and may synthesize images without introducing artifacts. Image artifacts may be explained by poor signal quality, magnitude smaller than one in a subset of voxels, or noise/distortion correction post image acquisition leading to voxels with very low signal intensity. In particular, mono-exponential models fail to correctly represent voxels with low signal intensity due to exponential fitting. Smoother images could be created by censoring those voxels by interpolating from surrounding voxels, smoothing low *b*-value images prior to calculation, or by thresholding low intensity voxels. For quantitative imaging, the details of such decisions would need to be clearly described and accounted for, and potentially could lead to more false positive/negative detections. Such enhanced images would not represent the measured truth and would include some unreliable voxels, which must be taken into consideration when interpreting the images. A “nicer looking” image does not necessarily mean that the image quality or reliability is better.

Prior studies reported sDWI to have higher subjective quality and tumor conspicuity^{5,27}. This may reflect the particular imaging sequences and, platforms used, or the particular image enhancement effects. It is also important to note that these prior results were mostly subjective judgements and not quantitative assessments of accuracy. In the presented study we have proven that tumor conspicuity is quantitatively greater with aDWI (CNR = 0.95) in comparison to sDWI (CNR = 0.65-0.84). Another option to improve sDWI is to use a multi-compartment DWI

model, e.g., RSIs, for a more stable and accurate signal extrapolation. For example, RSIs outperformed both sDWI and aDWI in the present study. Other promising multi-compartment models have proved to be superior to conventional multiparametric MRI, like a biomarker derived from VERDICT that outperformed ADC in the detection of csPCa¹⁴. Hybrid multidimensional MRI acquisitions also showed promising results for classifying csPCa with a reported AUC of 0.94³⁴.

One limiting factor of our study was that we only considered a retrospective dataset from a single scanner and a single institution. Further, only the conventional mono-exponential model was tested in the presented study. A precise comparison of all possible methods for synthesizing DWI is beyond the scope of this manuscript. RSIs is one quantitative biomarker based on a multi-compartment model. The acquisition protocol in the datasets here was not optimized for models like hybrid multi-dimensional MRI or VERDICT.

Conclusion

Within the prostate, sDWI is a systematically inaccurate representation of aDWI, but the techniques are quantitatively comparable in terms of detecting csPCa. In the surrounding pelvic tissue, high signal intensity artifacts are introduced with sDWI. These artifacts decrease the csPCa detection rate in surrounding tissues and might mask potential metastases within the pelvis. RSIs is superior to either sDWI or aDWI for quantitative csPCa detection. Despite the quantitative inaccuracies, sDWI may still be adequate for current subject clinical interpretation within the prostate.

References

1. Turkbey B, Rosenkrantz AB, Haider MA, et al. Prostate Imaging Reporting and Data System Version 2.1: 2019 Update of Prostate Imaging Reporting and Data System Version 2. *Eur Urol*. 2019;76(3):340-351. doi:10.1016/j.eururo.2019.02.033
2. Tang L, Zhou XJ. Diffusion MRI of Cancer: from Low to High b-Values. *J Magn Reson Imaging JMRI*. 2019;49(1):23-40. doi:10.1002/jmri.26293
3. Park MJ, Kim YK, Choi S youn, Rhim H, Lee WJ, Choi D. Preoperative detection of small pancreatic carcinoma: value of adding diffusion-weighted imaging to conventional MR imaging for improving confidence level. *Radiology*. 2014;273(2):433-443. doi:10.1148/radiol.14132563
4. Weinreb JC, Barentsz JO, Choyke PL, et al. PI-RADS Prostate Imaging - Reporting and Data System: 2015, Version 2. *Eur Urol*. 2016;69(1):16-40. doi:10.1016/j.eururo.2015.08.052
5. Jendoubi S, Wagner M, Montagne S, et al. MRI for prostate cancer: can computed high b-value DWI replace native acquisitions? *Eur Radiol*. 2019;29(10):5197-5204. doi:10.1007/s00330-019-06085-z
6. Shinmoto H, Oshio K, Tanimoto A, et al. Biexponential apparent diffusion coefficients in prostate cancer. *Magn Reson Imaging*. 2009;27(3):355-359. doi:10.1016/j.mri.2008.07.008
7. Karunamuni RA, Kuperman J, Seibert TM, et al. Relationship between kurtosis and bi-exponential characterization of high b-value diffusion-weighted imaging: application to prostate cancer. *Acta Radiol Stockh Swed 1987*. 2018;59(12):1523-1529. doi:10.1177/0284185118770889
8. Riches SF, Hawtin K, Charles-Edwards EM, de Souza NM. Diffusion-weighted imaging of the prostate and rectal wall: comparison of biexponential and monoexponential modelled diffusion and associated perfusion coefficients. *NMR Biomed*. 2009;22(3):318-325. doi:10.1002/nbm.1328
9. Le Bihan D, Breton E, Lallemand D, Aubin ML, Vignaud J, Laval-Jeantet M. Separation of diffusion and perfusion in intravoxel incoherent motion MR imaging. *Radiology*. 1988;168(2):497-505. doi:10.1148/radiology.168.2.3393671
10. Rosenkrantz AB, Sigmund EE, Johnson G, et al. Prostate Cancer: Feasibility and Preliminary Experience of a Diffusional Kurtosis Model for Detection and Assessment of Aggressiveness of Peripheral Zone Cancer. *Radiology*. 2012;264(1):126-135. doi:10.1148/radiol.12112290
11. Si Y, Liu RB. Diagnostic Performance of Monoexponential DWI Versus Diffusion Kurtosis Imaging in Prostate Cancer: A Systematic Review and Meta-Analysis. *AJR Am J Roentgenol*. 2018;211(2):358-368. doi:10.2214/AJR.17.18934
12. Panagiotaki E, Chan RW, Dikaios N, et al. Microstructural characterization of normal and malignant human prostate tissue with vascular, extracellular, and restricted diffusion for

- cytometry in tumours magnetic resonance imaging. *Invest Radiol*. 2015;50(4):218-227. doi:10.1097/RLI.0000000000000115
13. Johnston EW, Bonet-Carne E, Ferizi U, et al. VERDICT MRI for Prostate Cancer: Intracellular Volume Fraction versus Apparent Diffusion Coefficient. *Radiology*. 2019;291(2):391-397. doi:10.1148/radiol.2019181749
 14. Singh S, Rogers H, Kanber B, et al. Avoiding Unnecessary Biopsy after Multiparametric Prostate MRI with VERDICT Analysis: The INNOVATE Study. *Radiology*. Published online August 2, 2022:212536. doi:10.1148/radiol.212536
 15. Chatterjee A, Watson G, Myint E, Sved P, McEntee M, Bourne R. Changes in Epithelium, Stroma, and Lumen Space Correlate More Strongly with Gleason Pattern and Are Stronger Predictors of Prostate ADC Changes than Cellularity Metrics. *Radiology*. 2015;277(3):751-762. doi:10.1148/radiol.2015142414
 16. Sadinski M, Karczmar G, Peng Y, et al. Pilot Study of the Use of Hybrid Multidimensional T2-Weighted Imaging-DWI for the Diagnosis of Prostate Cancer and Evaluation of Gleason Score. *AJR Am J Roentgenol*. 2016;207(3):592-598. doi:10.2214/AJR.15.15626
 17. Chatterjee A, Bourne RM, Wang S, et al. Diagnosis of Prostate Cancer with Noninvasive Estimation of Prostate Tissue Composition by Using Hybrid Multidimensional MR Imaging: A Feasibility Study. *Radiology*. 2018;287(3):864-873. doi:10.1148/radiol.2018171130
 18. Lee GH, Chatterjee A, Karademir I, et al. Comparing Radiologist Performance in Diagnosing Clinically Significant Prostate Cancer with Multiparametric versus Hybrid Multidimensional MRI. *Radiology*. Published online July 26, 2022:211895. doi:10.1148/radiol.211895
 19. Brunsing RL, Schenker-Ahmed NM, White NS, et al. Restriction spectrum imaging: An evolving imaging biomarker in prostate MRI. *J Magn Reson Imaging*. 2017;45(2):323-336. doi:10.1002/jmri.25419
 20. Conlin CC, Feng CH, Rodriguez-Soto AE, et al. Improved Characterization of Diffusion in Normal and Cancerous Prostate Tissue Through Optimization of Multicompartmental Signal Models. *J Magn Reson Imaging*. 2021;53(2):628-639. doi:10.1002/jmri.27393
 21. Feng CH, Conlin CC, Batra K, et al. Voxel-level Classification of Prostate Cancer on Magnetic Resonance Imaging: Improving Accuracy Using Four-Compartment Restriction Spectrum Imaging. *J Magn Reson Imaging*. 2021;54(3):975-984. doi:10.1002/jmri.27623
 22. Zhong AY, Digma LA, Hussain T, et al. Automated Patient-level Prostate Cancer Detection with Quantitative Diffusion Magnetic Resonance Imaging. *Eur Urol Open Sci*. 2023;47:20-28. doi:10.1016/j.euros.2022.11.009
 23. Liu G, Lu Y, Dai Y, et al. Comparison of mono-exponential, bi-exponential, kurtosis, and fractional-order calculus models of diffusion-weighted imaging in characterizing prostate lesions in transition zone. *Abdom Radiol*. 2021;46(6):2740-2750. doi:10.1007/s00261-020-02903-x

24. Maas MC, Fütterer JJ, Scheenen TWJ. Quantitative evaluation of computed high B value diffusion-weighted magnetic resonance imaging of the prostate. *Invest Radiol*. 2013;48(11):779-786. doi:10.1097/RLI.0b013e31829705bb
25. Sahoo P, Rockne RC, Jung A, Gupta PK, Rathore RKS, Gupta RK. Synthetic Apparent Diffusion Coefficient for High b-Value Diffusion-Weighted MRI in Prostate. *Prostate Cancer*. 2020;2020:5091218. doi:10.1155/2020/5091218
26. Blackledge MD, Leach MO, Collins DJ, Koh DM. Computed Diffusion-weighted MR Imaging May Improve Tumor Detection. *Radiology*. 2011;261(2):573-581. doi:10.1148/radiol.11101919
27. Bittencourt LK, Attenberger UI, Lima D, et al. Feasibility study of computed vs measured high b-value (1400 s/mm²) diffusion-weighted MR images of the prostate. *World J Radiol*. 2014;6(6):374-380. doi:10.4329/wjr.v6.i6.374
28. White NS, McDonald C, McDonald CR, et al. Diffusion-weighted imaging in cancer: physical foundations and applications of restriction spectrum imaging. *Cancer Res*. 2014;74(17):4638-4652. doi:10.1158/0008-5472.CAN-13-3534
29. Holland D, Kuperman JM, Dale AM. Efficient correction of inhomogeneous static magnetic field-induced distortion in Echo Planar Imaging. *NeuroImage*. 2010;50(1):175-183. doi:10.1016/j.neuroimage.2009.11.044
30. Zhuang J, Hrabe J, Kangarlu A, et al. Correction of eddy-current distortions in diffusion tensor images using the known directions and strengths of diffusion gradients. *J Magn Reson Imaging*. 2006;24(5):1188-1193. doi:10.1002/jmri.20727
31. Hintze JL, Nelson RD. Violin Plots: A Box Plot-Density Trace Synergism. *Am Stat*. 1998;52(2):181-184. doi:10.1080/00031305.1998.10480559
32. DelPriore MR, Biswas D, Hippe DS, et al. Breast Cancer Conspicuity on Computed Versus Acquired High b-Value Diffusion-Weighted MRI. *Acad Radiol*. 2021;28(8):1108-1117. doi:10.1016/j.acra.2020.03.011
33. Conlin CC, Feng CH, Rodriguez-Soto AE, et al. Improved Characterization of Diffusion in Normal and Cancerous Prostate Tissue Through Optimization of Multicompartmental Signal Models. *J Magn Reson Imaging JMRI*. 2021;53(2):628-639. doi:10.1002/jmri.27393
34. Chatterjee Aritick. Validation of Prostate Tissue Composition by Using Hybrid Multidimensional MRI: Correlation with Histologic Findings. doi:10.1148/radiol.2021204459

Table 1 Acquisition parameters for clinical multi-parametric MRI; DWI = diffusion-weighted imaging; T2W = T_2 weighted MRI

Series	DWI	T2W
FOV [mm]	240*120	320*320
Matrix (resampled dimensions)	96*48 (128*64)	320*320 (512*512)
Number of Slices	16	32
Slice thickness [mm]	6	3
TR [ms]	4500	6080
TE [ms]	68	102
<i>b</i> -values [s/mm ²] (number of samples)	0 (2), 500 (6), 1000 (6), 2000 (12)	N/A

Table 2 Patient Characteristics range Q₁-Q₃= Range between lower first quartile to upper third quartile; csPCa = clinically significant prostate cancer. MRI = magnet resonance imaging; PSA = prostate-specific antigen

Parameter	Specification	Value
Number of patients	Total	151
Age [a]	Median (range Q ₁ -Q ₃)	66 (59-72)
Time from MRI to biopsy [d]	Median (range Q ₁ -Q ₃)	16 (1-35)
PSA at time of MRI [ng/ml]	Median (range Q ₁ -Q ₃)	7.3 (5.3-10.4)
Prostate volume [ml]	Median (range Q ₁ -Q ₃)	45 (34-61)
PSA density [ng/ml ²]	Median (range Q ₁ -Q ₃)	0.16 (0.11-0.25)
Best available pathology	Systematic	7
	Targeted	17
	Systematic and Targeted	85
	Prostatectomy	42
Targeted Biopsy	TRUS Guided	139
	Transperineal	9
	NaN	3
PI-RADS Score (csPCa)	I	0
	II	5 (3)
	III	27 (4)
	IV	55 (25)
	V	64 (54)
Gleason Grade Group	Benign	25
	1	40
	2	38
	3	20
	4	16
	5	12
Clinical Tumor stage	Negative Biopsy	25
	T1c	94
	T2a	13
	T2b	11
	T2c	8

Table 3 Summary of median differences between synthesized (sDWI) and acquired (aDWI) diffusion-weighted imaging. Comparison between sDWI and aDWI is presented relative to aDW. FOV= field of view

ROI	Datasets	Median Difference ± Interquartile range		
		Total (N = 151)	csPCA (N = 86)	Benign (N = 65)
Prostate	sDWI ₁₀₀₀ vs. aDWI	-55±27%	-52±29%	-59±22%
	sDWI ₅₀₀ vs. aDWI	-72±15%	-69±18%	-74±13%
Prostate+5 mm margin	sDWI ₁₀₀₀ vs. aDWI	-55±26%	-53±29%	-58±21%
	sDWI ₅₀₀ vs. aDWI	-72±18%	-69±19%	-74±13%
Prostate+30 mm margin	sDWI ₁₀₀₀ vs. aDWI	-48±35%	-46±41%	-50±28%
	sDWI ₅₀₀ vs. aDWI	-58±34%	-54±45%	-61±23%
Prostate+70 mm margin	sDWI ₁₀₀₀ vs. aDWI	1.9e19±4.1e19%	1.8e19±3.8e19%	2.0e19±6.4e19%
	sDWI ₅₀₀ vs. aDWI	1.5e47±1.7e48%	1.4e47±1.2e48%	1.5e47±3.0e48%
Whole FOV	sDWI ₁₀₀₀ vs. aDWI	1.1e19±2.3e19%	1.1e19±2.2e19%	1.6e19±2.5e19%
	sDWI ₅₀₀ vs. aDWI	3.4e48±8.9e50%	2.0e48±7.1e50%	1.3e49±9.2e50%

Table 4 Classification accuracy for the detection of cancer is shown for the prostate, prostate plus a 5 mm margin and the whole field of view (FOV). For statistical comparison bootstrapping (N=10,000) was performed and the 95% confidence intervals (CI) of AUC and the mean false positive rate at 90% sensitivity (FPR90) reported. ROI = Region of interest; AUC = area under the curve; RSirs = biomarker based on restriction spectrum imaging; aDWI = acquired diffusion b=2000 s/mm² MRI; sDWI₁₀₀₀ = synthesized image using acquired b-values up to 1000s/mm²; sDWI₅₀₀ = synthesized image using acquired b-values up to 500 s/mm²; * significantly different with p < 0.05 in comparison to each of the other metrics

Rol	Dataset	AUC	95th CI	FPR90
Prostate	RSirs	0.78*	0.71-0.86	0.50*
	aDWI	0.62	0.53-0.71	0.82
	sDWI ₁₀₀₀	0.65	0.56-0.73	0.76
	sDWI ₅₀₀	0.63	0.54-0.72	0.76
Prostate + 5 mm margin	RSirs	0.77*	0.68-0.84	0.53*
	aDWI	0.61	0.51-0.69	0.87
	sDWI ₁₀₀₀	0.60	0.51-0.69	0.84
	sDWI ₅₀₀	0.56	0.47-0.65	0.84
Prostate + 30 mm margin	RSirs	0.72*	0.64-0.80	0.62*
	aDWI	0.58	0.49-0.67	0.89
	sDWI ₁₀₀₀	0.52	0.43-0.61	0.83
	sDWI ₅₀₀	0.51	0.42-0.61	0.86
Prostate + 70 mm margin	RSirs	0.72*	0.64-0.81	0.61*
	aDWI	0.60	0.50-0.69	0.88
	sDWI ₁₀₀₀	0.46	0.36-0.55	0.87
	sDWI ₅₀₀	0.45	0.36-0.55	0.89
Whole FOV	RSirs	0.70*	0.61-0.78	0.62*
	aDWI	0.59*	0.49-0.68	0.90
	sDWI ₁₀₀₀	0.45	0.36-0.54	0.91
	sDWI ₅₀₀	0.47	0.38-0.56	0.90

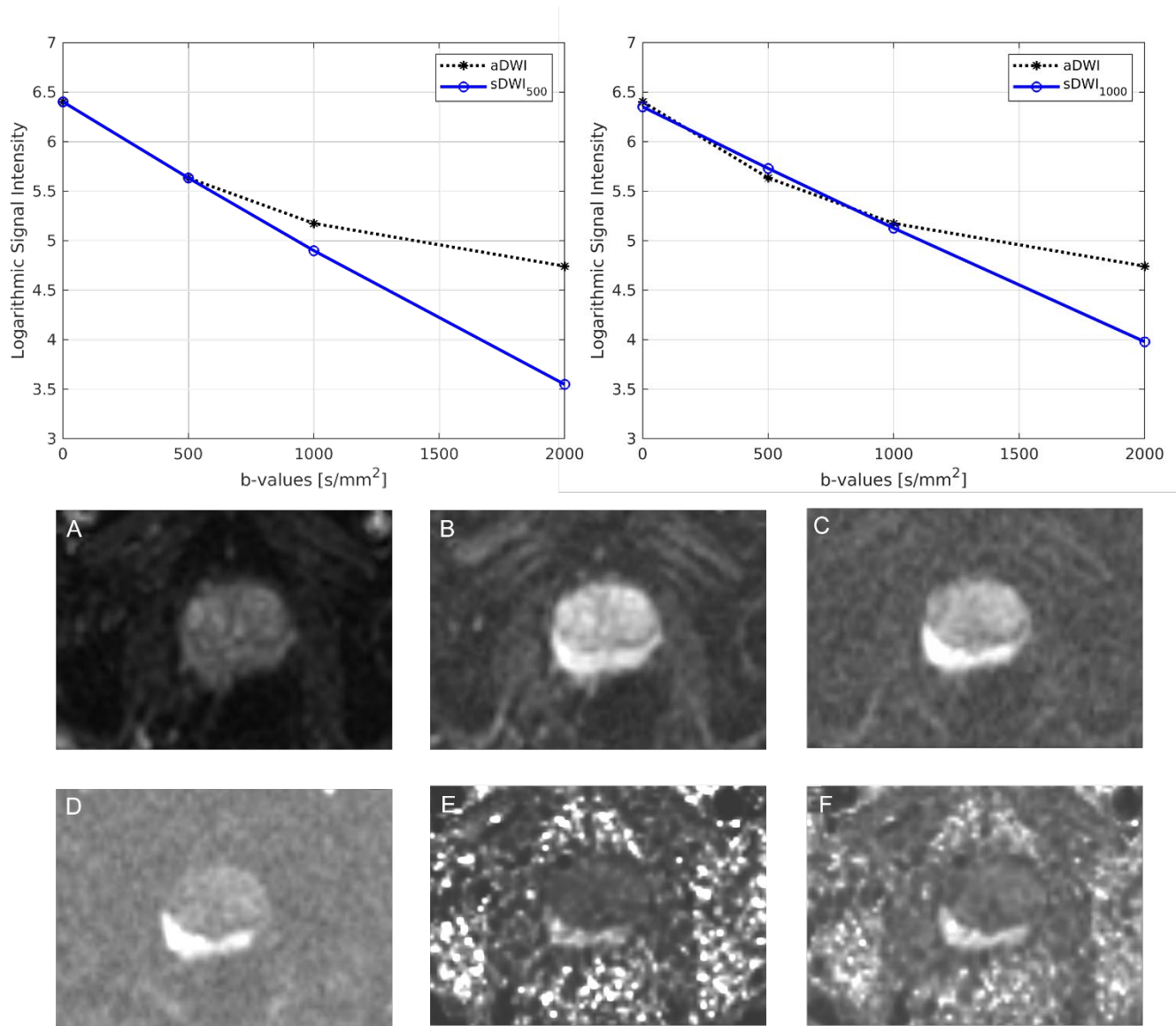


Figure 1. Comparison of acquired images to those synthesized with mono-exponential models using either b -values up to 500 s/mm^2 ($sDWI_{500}$) or b -values up to 1000 s/mm^2 ($sDWI_{1000}$) presented for one representative patient. Mean value within the prostate are compared. $sDWI$ is not an accurate representation of $aDWI$ at $b=2000$. Figures A-F show the different diffusion images for one patient. A-D present the acquired images for $b=0 \text{ s/mm}^2$ (A), $b=500 \text{ s/mm}^2$ (B), $b=1000 \text{ s/mm}^2$ (C) and $b=2000 \text{ s/mm}^2$ (D). E and F show the synthesized $b=2000 \text{ s/mm}^2$ images. E shows $sDWI_{500}$ and F $sDWI_{1000}$. $aDWI$ = acquired diffusion-weighted image for $b=2000 \text{ s/mm}^2$

a

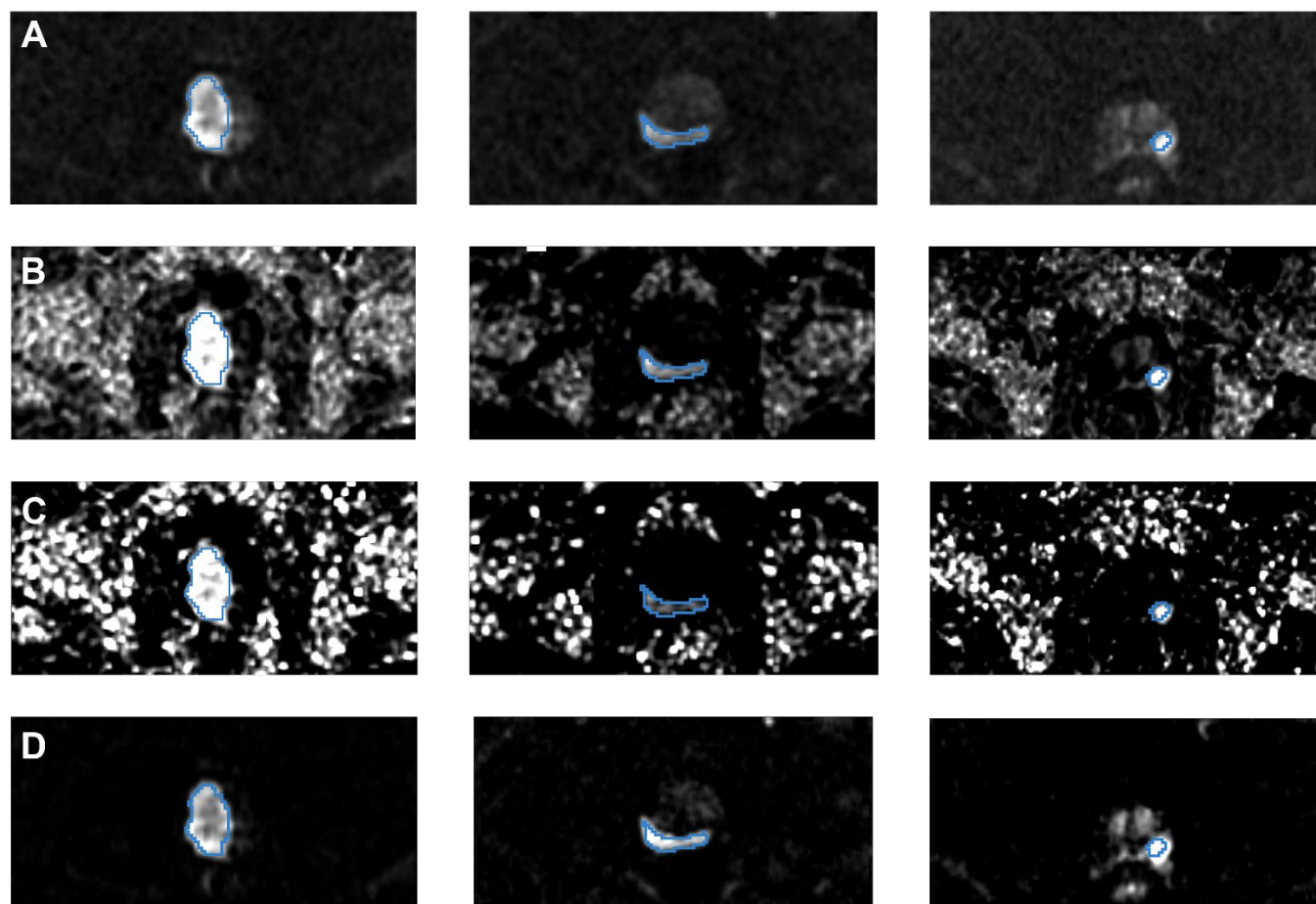


Figure 2. Representative images from three patients (corresponding to three columns). (A) acquired diffusion-weighted image (aDWI) for $b=2000$ s/mm², (B) synthesized DWI using acquired b -values up to $b=1000$ s/mm² (sDWI₁₀₀₀), (C) synthesized DWI using acquired values up to $b=500$ s/mm² (sDWI₅₀₀), and (D) restriction spectrum imaging restriction score (RSIrs). The radiologist-defined cancer lesion for each patient is indicated in blue. All presented patients had a PI-RADS score of 5. The same window level was chosen for all presented images.

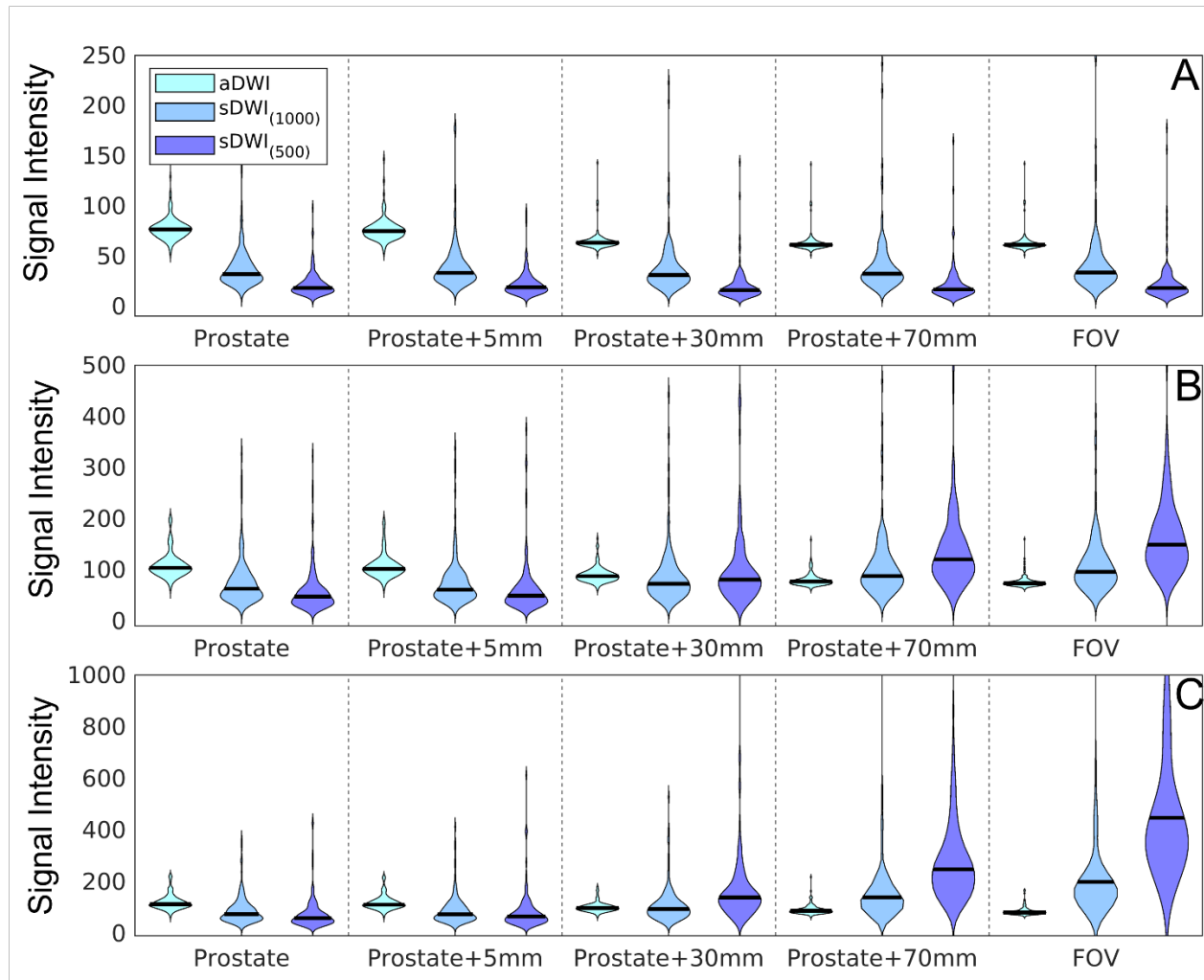


Figure 3. Violin plots summarizing the signal intensity across 151 patients for (A) 50th percentile, (B) 95th percentile, (C) and 98th percentiles of various DWI metrics calculated for each patient. The percentiles are estimated over different regions of interest: the prostate; the prostate with varying margin (5 mm, 30 mm, or 70 mm); and the whole field of view. aDWI = acquired diffusion-weighted image with $b=2000$ s/mm²; sDWI = synthesized DWI for $b=2000$ s/mm² using either acquired b -values up to 1000 s/mm² (sDWI₁₀₀₀) or up to 500 s/mm² (sDWI₅₀₀).

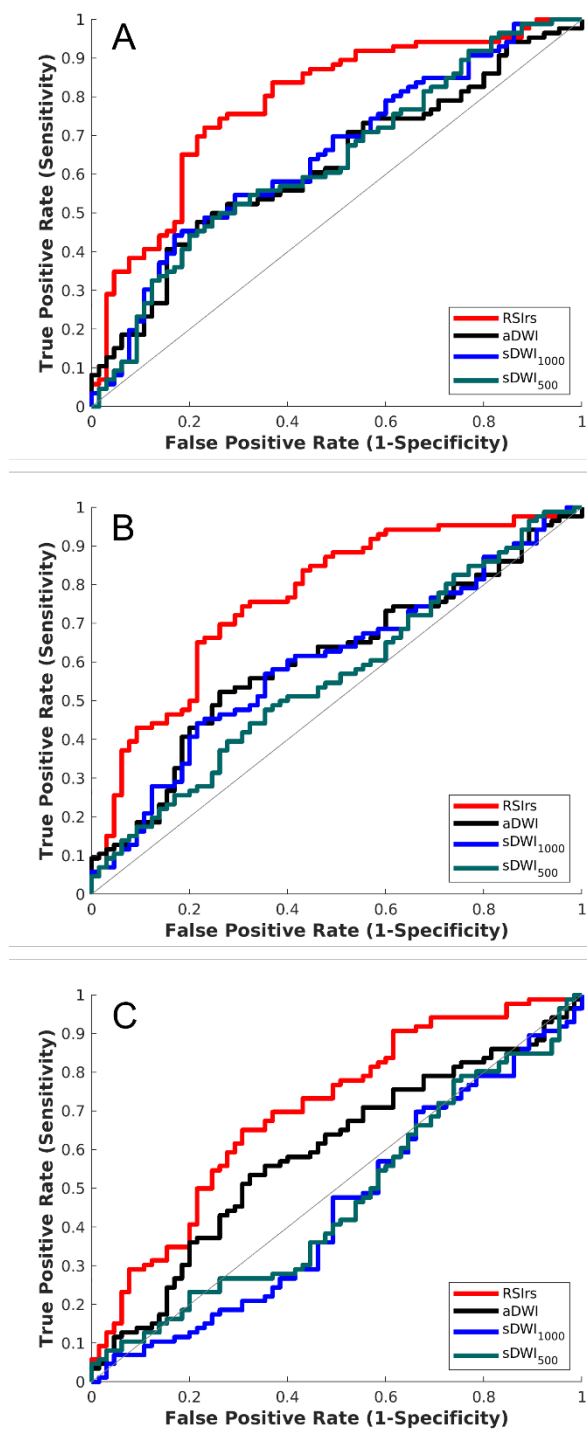


Figure 4. ROC curves for DWI metrics within three ROIs (A) the prostate, (B) the prostate with 5 mm margin, and (C) the whole field of view. The DWI metrics compared for classification accuracy are RSIs, acquired diffusion-weighted images (aDWI), synthesized DWI using b-values up to 1000 s/mm² (sDWI₁₀₀₀), and synthesized DWI using b-values up to 500 s/mm² (sDWI₅₀₀). Clinically significant prostate cancer was defined as a Gleason score ≥ 2 .

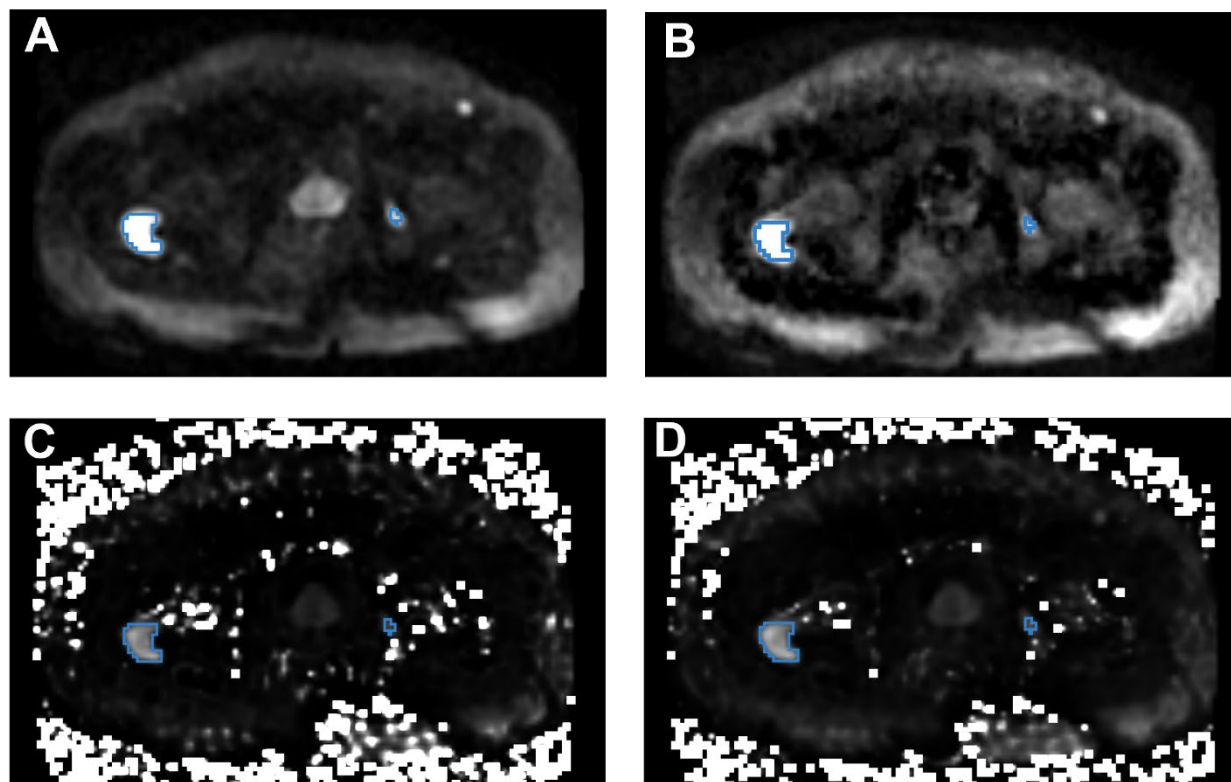


Figure 5. An example of pelvic DWI in a patient with prostate cancer bone metastases. The blue contours mark the cancer lesions. (A) acquired DWI with $b=2000 \text{ s/mm}^2$; (B) RSIs based on restriction spectrum imaging; (C) synthesized DWI using acquired b -values up to 500 s/mm^2 ; and (D) synthesized DWI using acquired b -values up to 1000 s/mm^2 . Tumor lesions are easily detectable in A and B, but there is more high-intensity artifact on sDWI, and the smaller bone metastasis is not as easily identifiable in C and D.